

A Comparative Study of Carrier-Frequency Modulation Techniques for Conducted EMI Suppression in PWM Converters

K. K. Tse, *Associate Member, IEEE*, Henry Shu-Hung Chung, *Member, IEEE*, S. Y. Ron Hui, *Senior Member, IEEE*, and H. C. So, *Member, IEEE*

Abstract—A rigorous mathematical analysis and a comparative study of carrier-frequency modulation (CFM) techniques for the conducted electromagnetic interference (EMI) suppression in pulsedwidth-modulated converters is presented. CFM techniques dither the switching period with a small amplitude variation around the nominal value, so that the harmonic power is redistributed over the spectrum of concern. Two types of dithering signals, including the periodic and random signals, are investigated in this paper. The operational characteristics as well as the input and output power spectra of the converters with the two modulating signals are compared. In particular, their characteristics in the low- and high-frequency harmonic power redistribution will be depicted. It is shown that random CFM (RCFM) gives a more effective way to disperse the harmonics around the switching frequency than the periodic CFM (PCFM) with the same frequency deviation. However, RCFM introduces higher low-frequency harmonics than the PCFM at the converter output. Furthermore, effects of the resolution filter bandwidth in the electromagnetic compatibility analyzer on conducted EMI measurement is discussed. The validity of the analyses is confirmed experimentally by using a dc/dc buck converter operating in continuous conduction mode.

Index Terms—DC–DC power conversion, power electronics, pulsedwidth modulation, random switching techniques, switching circuits.

I. INTRODUCTION

AS THE electromagnetic spectrum becomes crowded, many countries have imposed electromagnetic compatibility (EMC) regulations that must be met before electronic products can be sold legally. The most direct way of solving electromagnetic interference (EMI) problems is to reduce the emission from the noise source [1].

EMI is a serious problem in power electronics circuits because of their fast switching characteristics. Extensive research has been conducted on developing various soft-switching techniques for different applications to reduce both switching

loss and radiated EMI [2]. By smoothing the switching transients and reducing the ringing problems, radiated EMI emission can be lessened. Although those techniques are particularly effective for reducing high-frequency emissions, they are unsuitable for suppressing switching-frequency-related emissions (i.e., conducted EMI). Apart from using passive noise filters and shields in the circuit, another approach of EMI suppression is based on modulating a parameter, such as the switching frequency, pulsewidth, or pulse position, of the pulsedwidth-modulated (PWM) signals that apply to the switching devices either in a periodic [3] or random manner [4]–[8]. The parameter is dithered with small amplitudes around the nominal value, so that the harmonic power is redistributed over the spectrum of concern. Among all possible parameters, modulating the frequency, namely, the carrier-frequency modulation (CFM), is a very effective solution because the switching frequency is not fixed at a constant value and, thus, the spectral component at the original switching frequency will be diminished in the input and output spectra.

As reported in [3], periodic CFM (PCFM) can reduce the conducted EMI with a suitable selection of the modulating frequency. This method introduces sidebands at the original discrete frequency components in the standard PWM scheme with much smaller magnitude. So far, effects of the resolution filter bandwidth in the EMC analyzer on the discrepancies between theoretical and measured spectra have not been addressed. Moreover, as discussed in [3], Carson's rule is inapplicable for studying high-frequency behaviors, due to the overlap of the sideband harmonics of different switching frequency harmonics. In this paper, rigorous mathematical analysis of the spectra will be given.

For the random switching schemes, random CFM (RCFM) with fixed duty cycle is the best option because: 1) all discrete harmonics can be significantly reduced; 2) the harmonic power can be spread over as a continuous noise spectrum of small magnitude; and 3) the low-frequency harmonic injection is minimal [6].

This paper presents a comparative study of using PCFM and RCFM on the conducted EMI suppression in PWM converters. Issues addressed include the operational properties and the input and output power spectral densities of the converters with the two modulation techniques. In particular, their characteristics in low- and high-frequency harmonic power redistribution are depicted. The effects of the resolution filter bandwidth in the EMC analyzer on the conducted EMI measurement will be emphasized. The validity of the analyses is verified experimentally with a dc/dc buck converter.

Manuscript received October 2, 2000; revised November 26, 2001. Abstract published on the Internet March 7, 2002. This work was supported by the Research Grants Council of the Hong Kong Special Administrative Region, China, under CERF Project 9040266. The work of K. K. Tse was supported by The Croucher Foundation Fellowship.

K. K. Tse was with the Department of Electronic Engineering, City University of Hong Kong, Kowloon, Hong Kong. He is now with Johnson Electric, Hong Kong.

H. S.-H. Chung, S. Y. R. Hui, and H. C. So are with the Department of Electronic Engineering, City University of Hong Kong, Kowloon, Hong Kong (e-mail: eeshc@cityu.edu.hk).

Publisher Item Identifier S 0278-0046(02)04926-2.

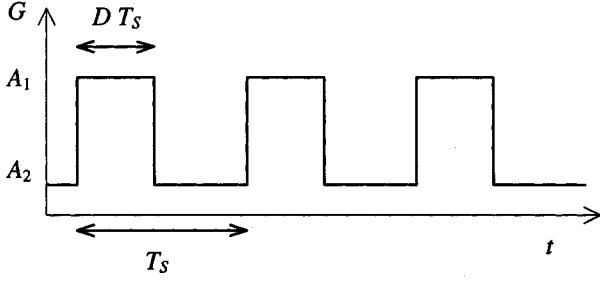


Fig. 1. Typical PWM function.

II. PCFM AND RCFM

Fig. 1 shows a typical PWM function $G(t)$ with the duty cycle D and the switching period T_s . $G(t)$ has two discrete levels (namely, A_1 and A_2), which are applicable to describe the behaviors of switching converters. Mathematically, $G(t)$ can be expressed by a Fourier series [9]

$$G(t) = \sum_{n=-\infty}^{\infty} C_n e^{j\theta_n} \quad (1)$$

where C_n and θ_n are the magnitude and phase of the n th harmonic, respectively.

C_n can be calculated by

$$\begin{aligned} C_n &= \frac{1}{T_s} \int_{-T_s/2}^{T_s/2} G(t) e^{-j2\pi n f t} dt \\ &= \frac{j}{2\pi n f T_s} [A_1 (e^{-j2\pi n f D T} - 1) \\ &\quad + A_2 (e^{-j2\pi n f T} - e^{-j2\pi n f D T})]. \end{aligned} \quad (2)$$

A. Theoretical Power Spectrum With PCFM

With the PCFM, the switching frequency of $G(t)$ is modulated by a sinusoidal function of amplitude Δf_s and frequency f_m . In practice, Δf_s represents the maximum frequency deviation in the switching frequency and f_m is the modulating frequency. The instantaneous frequency $f_{\text{inst},n}$ of the n th harmonic is equal to the time derivative of θ_n . That is,

$$\begin{aligned} f_{\text{inst},n} &= \frac{1}{2\pi} \cdot \frac{d\theta_n}{dt} \\ &= n[f_s + \Delta f_s \cos(2\pi f_m t)] \end{aligned} \quad (3)$$

where $f_s = 1/T_s$ is the nominal switching frequency.

By using (3),

$$\begin{aligned} \theta_n &= 2\pi n \int_0^t [f_s + \Delta f_s \cos(2\pi f_m \lambda)] d\lambda \\ &= 2\pi n f_s t + n\beta \sin(2\pi f_m t) \end{aligned} \quad (4)$$

where β is the ratio of the peak instantaneous frequency deviation to the frequency of the modulating signal, namely, the modulation index in [3] and [11]. It is defined as

$$\beta = \frac{\Delta f_s}{f_m}. \quad (5)$$

Substituting (4) into (1) gives

$$G(t) = \sum_{n=-\infty}^{\infty} C_n e^{jn2\pi f_s t} \{ \cos[n\beta \sin(2\pi f_m t)] + j \sin[n\beta \sin(2\pi f_m t)] \}. \quad (6)$$

By using the Jacobi equations in [10], the cosine and sine terms in (6) can be expressed as

$$\begin{aligned} \cos[n\beta \sin(2\pi f_m t)] &= J_0(n\beta) \\ &\quad + \sum_{k=\text{even}}^{\infty} 2J_k(n\beta) \cos(2\pi k f_m t) \\ \sin[n\beta \sin(2\pi f_m t)] &= \sum_{k=\text{odd}}^{\infty} 2J_k(n\beta) \sin(2\pi k f_m t) \end{aligned} \quad (7)$$

where $J_k(\cdot)$ is the k th order Bessel function. It can be expanded by the following series:

$$\begin{aligned} J_k(n\beta) &= \left(\frac{n\beta}{2}\right)^k \left[\frac{1}{k!} - \frac{\left(\frac{n\beta}{2}\right)^2}{1!(k+1)!} \right. \\ &\quad \left. + \frac{\left(\frac{n\beta}{2}\right)^4}{2!(k+2)!} - \frac{\left(\frac{n\beta}{2}\right)^6}{3!(k+3)!} + \dots \right]. \end{aligned} \quad (8)$$

Numerical values of the Bessel functions with respect to $n\beta$ up to the tenth order are tabulated in Table I. The following two properties are also noted:

$$J_k(n\beta) \approx 0, \quad k > n\beta + 1, \quad (9a)$$

and

$$\sum_{k=-\infty}^{\infty} J_k^2(n\beta) = 1 \quad \forall n\beta. \quad (9b)$$

Substituting (7) into (6) gives

$$\begin{aligned} G(t) &= \sum_{n=-\infty}^{\infty} C_n e^{j2\pi n f_s t} \\ &\quad \times \left[J_0(n\beta) + \sum_{k=1}^{\infty} J_k(n\beta) e^{j2\pi k f_m t} \right. \\ &\quad \left. + \sum_{k=\text{even}}^{\infty} J_k(n\beta) e^{-j2\pi k f_m t} \right. \\ &\quad \left. - \sum_{k=\text{odd}}^{\infty} J_k(n\beta) e^{-j2\pi k f_m t} \right] \\ &= \sum_{n=-\infty}^{\infty} C_n \left\{ J_0(n\beta) e^{j2\pi n f_s t} \right. \\ &\quad \left. + \sum_{k=1}^{\infty} J_k(n\beta) \left[e^{j2\pi(n f_s + k f_m)t} \right. \right. \\ &\quad \left. \left. + (-1)^k e^{j2\pi(n f_s - k f_m)t} \right] \right\}. \end{aligned} \quad (10)$$

TABLE I
NUMERICAL VALUES OF THE FIRST TEN ORDER J_k WITH RESPECT TO $n\beta$

$n\beta$	J_0	J_1	J_2	J_3	J_4	J_5	J_6	J_7	J_8	J_9
0	1.00	-	-	-	-	-	-	-	-	-
0.5	0.94	0.24	0.03	-	-	-	-	-	-	-
1	0.77	0.44	0.11	0.02	-	-	-	-	-	-
2	0.22	0.58	0.35	0.12	0.03	-	-	-	-	-
3	-0.26	0.34	0.49	0.31	0.13	0.04	0.01	-	-	-
4	-0.40	-0.07	0.36	0.43	0.28	0.13	0.05	0.02	-	-
5	-0.18	-0.33	0.05	0.36	0.39	0.26	0.13	0.05	0.02	-
6	0.15	-0.28	-0.24	0.11	0.36	0.36	0.25	0.13	0.06	0.02

The magnitude of $G(t)$ at frequency f , $G(f, \beta)$, can be shown to be

$$G(f, \beta) = \sum_{n=-\infty}^{\infty} C_n \left\{ J_0(n\beta) \delta(f - nf_s) + \sum_{k=1}^{\infty} J_k(n\beta) [\delta(f - nf_s - kf_m) + (-1)^k \delta(f - nf_s + kf_m)] \right\}. \quad (11)$$

Its power spectrum $S_G(f, \beta)$ in the positive frequency range is equal to

$$S_G(f, \beta) = 2 \left| \sum_{n=1}^{\infty} C_n \left\{ J_0(n\beta) \delta(f - nf_s) + \sum_{k=1}^{\infty} J_k(n\beta) [\delta(f - nf_s - kf_m) + (-1)^k \delta(f - nf_s + kf_m)] \right\} \right|^2, \quad f > 0. \quad (12)$$

Thus, $S_G(f, \beta)$ contains infinite discrete harmonics and is dependent on β and f_m .

For the standard PWM scheme (i.e., $\beta = 0$), $J_0(0)$ exists only. Referring to Table I, (12) becomes

$$S_G(f, \beta) = 2 \sum_{n=1}^{\infty} |C_n|^2 \delta(f - nf_s). \quad (13)$$

As expected, the power spectrum consists of the discrete harmonics at the multiples of f_s .

For the PCFM scheme (i.e., $\beta \neq 0$), $J_k(n\beta)$ leads to upper and lower sidebands at the multiples of f_s . Although the number of side frequencies is infinite, the bandwidth B_n of the sideband of the n th harmonic can be approximated by (9a) as

$$B_n = 2(n\beta + 1)f_m \quad (14)$$

where $B_n \in [nf_s - (n\beta + 1)f_m, nf_s + (n\beta + 1)f_m]$.

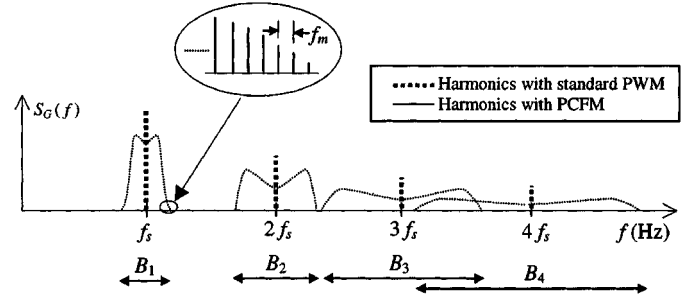


Fig. 2. Spectral structure of S_G with PCFM.

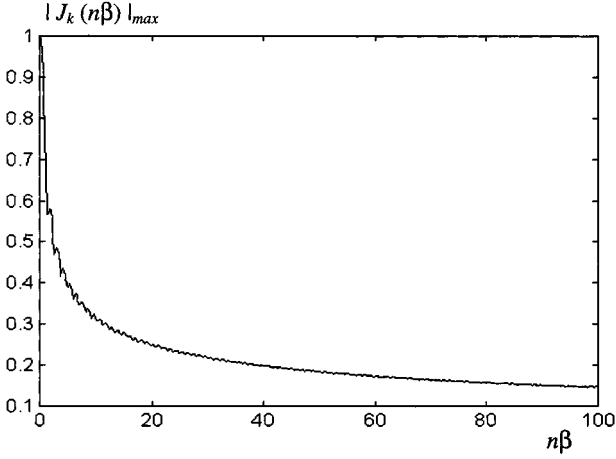
If $n\beta$ is sufficiently large, B_n can further be approximated by

$$B_n \approx 2n\beta f_m = 2n\Delta f_s, \quad \beta \gg 1. \quad (15)$$

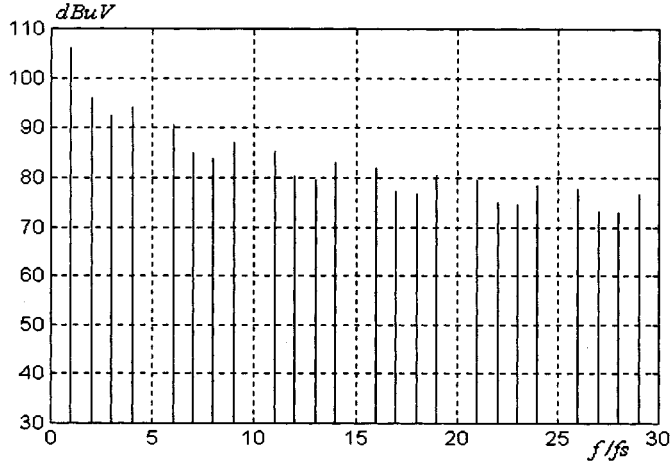
Compared with Carson's rule [3], (12) gives a more general formula that describes the spectrum of the PWM waveform. It is possible to study the spectrum at high-order switching harmonics and large Δf_s , in which case the side frequencies of different switching harmonics may overlap. As will be discussed in Section II-C, it is possible to predict accurately the measured power spectrum using (12).

Fig. 2 depicts the spectral structure of S_G . PCFM generates the upper and lower sidebands with the bandwidth B_n at the n th multiples of f_s . Each sideband consists of side frequencies, which are f_m apart and have magnitudes much smaller than the value at the center frequency in the standard PWM scheme. The number of side frequencies in B_n is equal to the order of J_k . Mathematically, using a larger value of β results in more side frequencies. As boldfaced in Table I, the maximum absolute values of J_k , $|J_k(n\beta)|_{\max}$, under each $n\beta$ determine the peak magnitude in the considered sideband. They give a relative measure on the harmonic reduction as compared to the standard PWM scheme. Fig. 3 shows the relationships of $|J_k(n\beta)|_{\max}$ against $n\beta$. Basically, $|J_k(n\beta)|_{\max}$ decreases as $n\beta$ increases. However, its rate of decrement decreases with the increase in $n\beta$. With the above phenomena, the following properties can be concluded.

- P1) Harmonic suppression effect increases with the increase in β .
- P2) Suppression of high-order harmonics is more effective than the low-order ones.
- P3) Insignificant enhancements in harmonic suppression are observed when $n\beta$ is sufficiently large.

Fig. 3. Relationships of $|J_k(n\beta)|_{\max}$ against $n\beta$.TABLE II
COMPONENT VALUES AND SPECIFICATIONS OF THE BUCK CONVERTER

Inductor	940μH	Output voltage	5V
Capacitor	4.7μF	Nominal switching frequency f_s	100kHz
Output Load	10Ω	Duty-cycle D	0.4

Fig. 4. Theoretical input current power spectrum with $\beta = 0$.

The above properties are illustrated with an example of a buck converter. Its specifications are tabulated in Table II. The values of A_1 and A_2 in Fig. 1 are 0.48 and 0 A, respectively, in the following analysis. Fig. 4 shows the theoretical input current power spectrum with β equals zero (i.e., standard PWM scheme). It contains discrete harmonics at the multiples of the switching frequency only. Figs. 5 and 6 show the power spectra with $\beta = 2$, $\beta = 8$, and $\beta = 16$, respectively, under two testing conditions.

The first testing condition is that f_m is fixed at 3 kHz with $\Delta f_s = 6$ kHz, $\Delta f_s = 24$ kHz, and $\Delta f_s = 48$ kHz. The results in Fig. 5 reveal that harmonic suppression is more effective with a larger β (i.e., $\beta = 8$ and $\beta = 16$). This confirms P1). Comparing Figs. 4 and 5(b) shows a reduction of 10 dB in

the low-frequency range and 20 dB in the high-frequency range. This confirms P2).

Fig. 6 shows the results in the second test when Δf_s equals 12 kHz with $f_m = 6$ kHz, $f_m = 1.5$ kHz, and $f_m = 750$ Hz, respectively. The results are similar to those in Fig. 5. They indicate that harmonic suppression is highly dependent on the value of β and is relatively independent on the combinations of f_m and Δf_s . Conversely, it will be shown later that the measured spectra are dependent on f_m and Δf_s , because of the interaction between the resolution filter in the EMC analyzer and S_G .

It can be observed that the results for $\beta = 16$ in Figs. 5(c) and 6(c) are similar to those of Figs. 5(b) and 6(b), respectively, especially at the high-frequency range. This demonstrates P3), that the spectra will be similar when $n\beta$ is sufficiently large.

B. Theoretical Power Spectral Density (PSD) With RCFM

For the RCFM, T_s in Fig. 1 is dithered in random manner and D is kept constant [6]. Instead of using power spectrum, PSD is considered in the analysis [5]. The PSD $S_G(f, \Re)$ under RCFM has been shown to be

$$S_G(f, \Re) = \frac{1}{E[T_k]} \left\{ E[|G(f)|^2] + 2\text{Re} \left\{ \frac{E[G(f)e^{j2\pi f T_k}]E[G^*(f)]}{1 - E[e^{j2\pi f T_k}]} \right\} \right\} \quad (16)$$

where $G^*(f)$ is the complex conjugate of $G(f)$ and T_k is the instantaneous switching period. The probability density function of T_k , $P(T_k)$, is of uniform distribution with the expected value of T_s . It is defined as

$$P(T_k) = \frac{1}{T_2 - T_1} = \frac{1}{\Re T_s} \quad (17)$$

where T_1 and T_2 are the minimum and maximum possible switching periods, respectively, and \Re is the randomness level.

This scheme spreads the discrete harmonics over the frequency spectrum. As \Re increases, the harmonics are gradually spread over. However, no significant improvements in spreading high-frequency harmonics are observed when \Re is larger than a certain value, such as 0.15 in [6]. Moreover, low-frequency harmonic components increase as \Re increases.

C. Discrepancies Between Theoretical and Measured Spectra

The bandwidth BW_{res} of the resolution filter in the EMC analyzer significantly affects the measured power spectrum. BW_{res} might introduce discrepancies between the theoretical and measured spectra. In the following discussions, the HP 8590EM series EMC analyzer is used for illustration.

As shown in [12], attenuation of the resolution filter is in Gaussian characteristics. The approximate ratio between the bandwidth at -60 dB (denoted by BW_{-60}) and BW_{res} is 15. That is,

$$\frac{BW_{-60}}{BW_{\text{res}}} \approx 15. \quad (18)$$

In order to predict the displayed spectrum on the EMC analyzer, a triangle-like filter response shown in Fig. 7 is proposed to

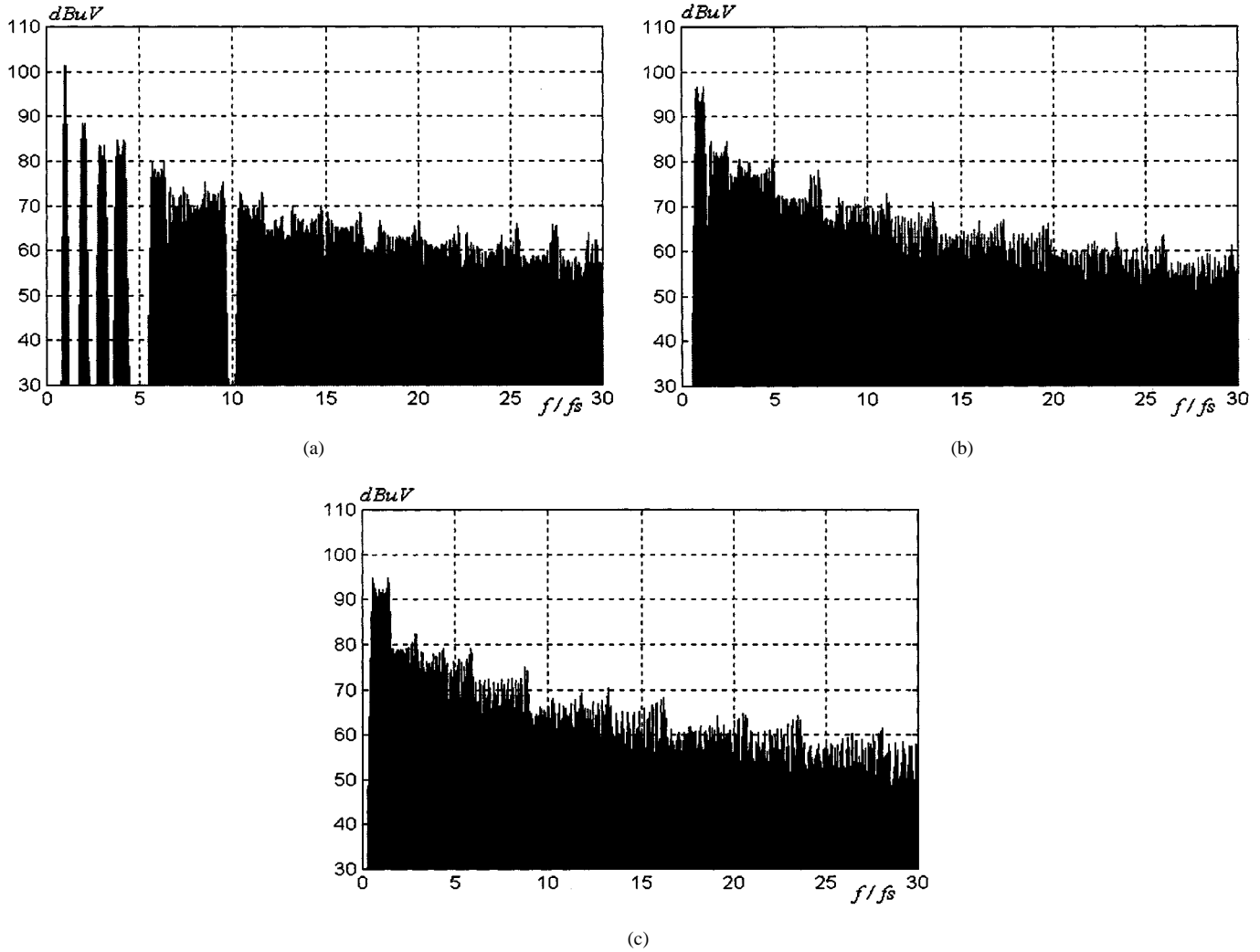


Fig. 5. Theoretical power spectra of the input current with $f_m = 3$ kHz. (a) $\Delta f_s = 6$ kHz and $\beta = 2$. (b) $\Delta f_s = 24$ kHz and $\beta = 8$. (c) $\Delta f_s = 48$ kHz and $\beta = 16$.

model the filter attenuation. The filter response function $W(f)$ is defined as follows:

$$W(f) = \begin{cases} W_R(f), & \text{for } f \geq f_0 \\ W_L(f), & \text{for } f \leq f_0 \end{cases} \quad (19)$$

where f_0 is the center frequency over BW_{res} , $W_R(f) = 10^{-(0.4/BW_{\text{res}})(f-f_0)} = -(4/BW_{\text{res}})(f - f_0)$ dB, and $W_L(f) = 10^{(0.4/BW_{\text{res}})(f-f_0)} = -(4/BW_{\text{res}})(f - f_0)$ dB.

Hence, the measured power at f_0 by the analyzer is equal to

$$\begin{aligned} S_{G,\text{meas}}(f_0, \beta) &= \int_{f_0-7.5BW_{\text{res}}}^{f_0+7.5BW_{\text{res}}} S_G(f, \beta) |W(f)|^2 df \\ &= S_G(f_0, \beta) \\ &\quad + \int_{f_0+\Delta}^{f_0+7.5BW_{\text{res}}} S_G(f, \beta) W_R(f)^2 df \\ &\quad + \int_{f_0-\Delta}^{f_0-7.5BW_{\text{res}}} S_G(f, \beta) W_L(f)^2 df \end{aligned} \quad (20)$$

where $\Delta \rightarrow 0$.

By using the property in (9b), the total power of the n th order harmonic in the fixed-frequency PWM scheme is equal to the sum of the discrete powers over B_n in PCFM. The number of side frequencies N_{sf} that falls within BW_{res} can be approximated by

$$N_{sf} = \frac{15BW_{\text{res}}}{f_m} = \frac{15BW_{\text{res}}}{\Delta f_s} \beta. \quad (21)$$

The measured spectrum will be similar to the theoretical calculation if N_{sf} is small. This can be achieved by either reducing BW_{res} or increasing f_m and Δf_s . According to some international EMC regulations, such as the Comite International Special des Perturbations Radioelectriques (CISPR), BW_{res} is fixed in the measurement. Thus, the most viable approach is to adjust f_m and Δf_s . However, if f_m is too large, β will be small and the magnitude of the side frequencies will increase. If Δf_s is too large, it will be discussed later that low-frequency harmonics will be introduced. Table III shows the interactions between S_G and the resolution filter under two testing conditions. First f_m is fixed. BW_{res} will enclose more harmonic power in S_G with

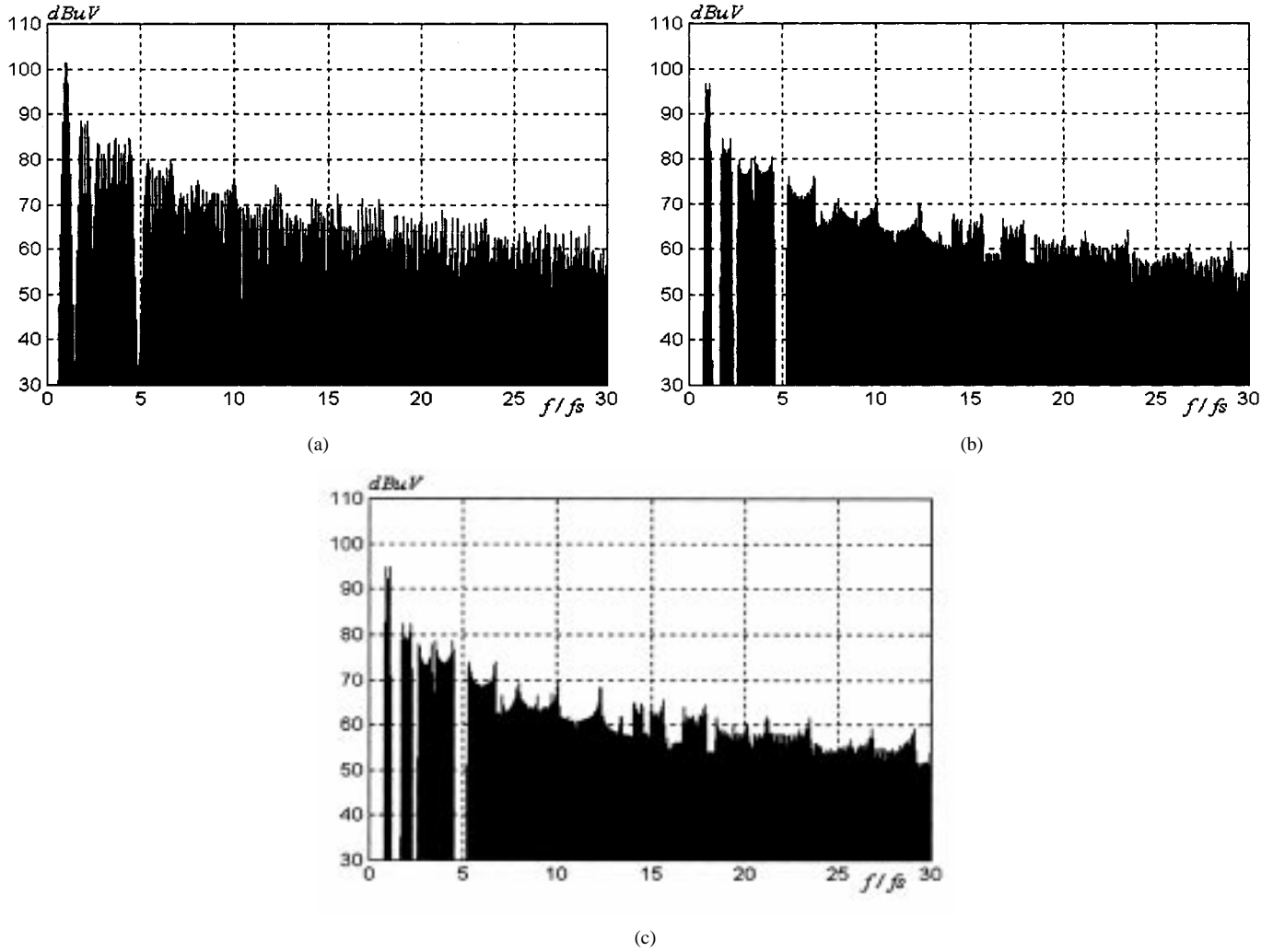


Fig. 6. Theoretical power spectra of the input current with $\Delta f_s = 12$ kHz. (a) $f_m = 6$ kHz and $\beta = 2$. (b) $f_m = 1.5$ kHz and $\beta = 8$. (c) $f_m = 750$ Hz and $\beta = 16$.

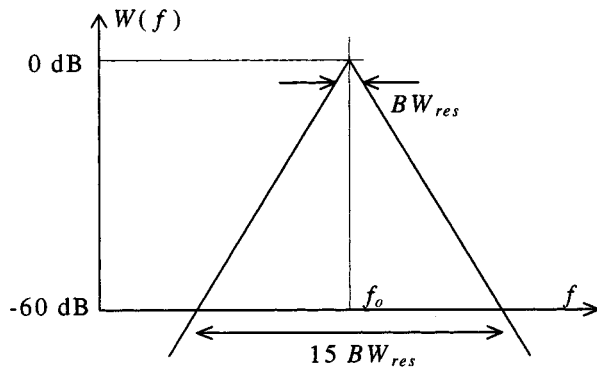


Fig. 7. Model of the triangle-like filter response in the EMC analyzer.

smaller β (i.e., small Δf_s). Second Δf_s is fixed. The measured S_G is insensitive to β . The measured spectrum is unable to differentiate the effectiveness of β in the actual EMI suppression.

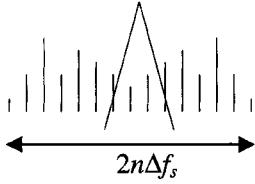



In order to demonstrate the above observations, the theoretical power spectra shown in Figs. 5 and 6 are used to compare the measured power spectra, which are calculated by (20). With BW_{res} equals 9 kHz, the measured power spectra for Figs. 5

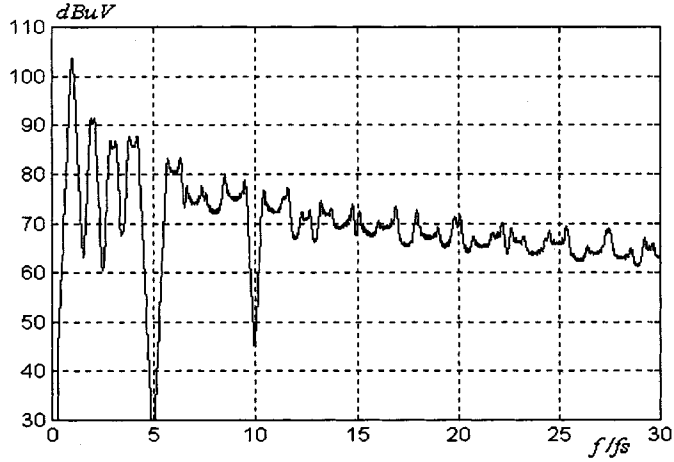
and 6 are shown in Figs. 8 and 9, respectively. As expected, the measured results are higher than the corresponding envelopes in Figs. 5 and 6. Comparing Fig. 8(a) with Fig. 8(b), the results vary with Δf_s (and, hence, β). Increasing Δf_s can effectively disperse the low-order harmonics. However, with the same Δf_s and different β in Fig. 9, the predicted results in the two cases are similar, confirming the argument of the discrepancies.

Finally, Δf_s is not a prime factor in high-frequency harmonic suppression in all cases. Since B_n increases with the harmonic order, the side frequencies in B_n will overlap inevitably with the lower band B_{n-1} . The overlapped regions increase the PSD over BW_{res} and become relatively insensitive to Δf_s . Conversely, since the overlapping effect is small at the low-order harmonics, the measured spectra vary with Δf_s (Fig. 8). Carson's rule can be applied to explain the EMI suppression with the increase in Δf_s [3].

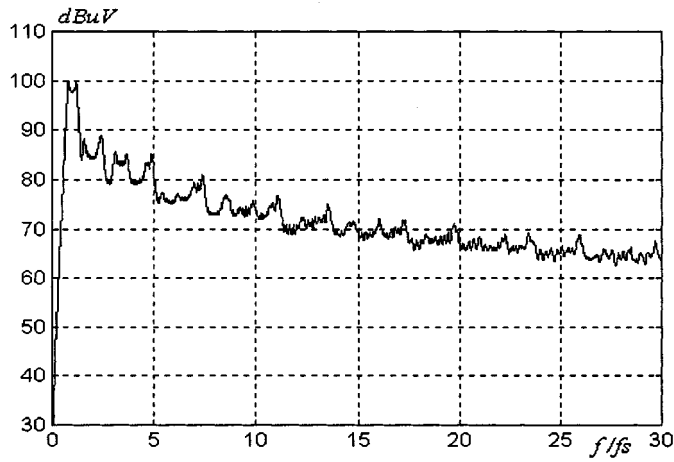
In the RCFM, as frequency components randomly appear, the measured spectrum is dependent on the spectral density inside BW_{res} . If \mathcal{R} is sufficiently large, the PSD of the measured PWM waveform is uniformly distributed. The measured spectrum will increase as BW_{res} increases.

TABLE III
INTERACTION OF THE n TH HARMONIC IN S_G WITH THE RESOLUTION FILTER

PCFM at	Low β	High β
Fixed f_m And Different Δf_s		
Different f_m and Fixed Δf_s		



(a)



(b)

Fig. 8. Comparison of the predicted power spectra with $BW_{rms} = 9$ kHz and $f_m = 3$ kHz. (a) $\Delta f_s = 6$ kHz and $\beta = 2$. (b) $\Delta f_s = 24$ kHz and $\beta = 8$.

D. Low-Frequency Noise

A dc/dc converter can be considered as a low-pass filter fed by different types of input sources [6]. Let $H(f)$ be the filter

transfer characteristic for buck and transimpedance for boost and buck-boost converters. The power spectrum of the noise output $S_{no}(f, \beta)$ is

$$S_{no}(f, \beta) = S_G(f, \beta) |H(f)|^2, \quad f \neq 0 \quad (22)$$

where S_G is the diode voltage for buck converters and inductor current for boost and buck-boost converters.

Since $|H(f)|^2$ rolls off at the high-frequency range, the rms value of noise ripple v_{no} can be approximated by

$$\begin{aligned} v_{no}(\beta) &= \left[\int_0^{2f_s} S_G(f, \beta) |H(f)|^2 df \right]^{1/2} \\ &\cong \left[\sum_{n=1}^2 \sum_{k=0}^{n\beta+1} |C_n J_k(n\beta) H(nf_s \pm kf_m)|^2 \right]^{1/2} \end{aligned} \quad (23)$$

for the PCFM.

As discussed above, the lower sideband of the first harmonic is subject to Δf_s . Using large Δf_s will introduce low-frequency noise at the converter output. In order to keep a tight output regulation, the lowest harmonic spectra in PCFM has to be far beyond the cutoff frequency f_{cutoff} of $H(f)$. Hence,

$$\Delta f_s \ll f_s - f_{cutoff}. \quad (24)$$

With the RCFM, it has been shown in [6] that the PSD of the output noise is

$$v_{no}(\Re) = \left[\frac{4f_s}{N} \sum_{k=1}^N S_G \left(\frac{2kf_s}{N}, \Re \right) \left| H \left(\frac{2kf_s}{N} \right) \right|^2 \right]^{1/2} \quad (25)$$

where N is the number of frequency points within $[0, 2f_s]$.

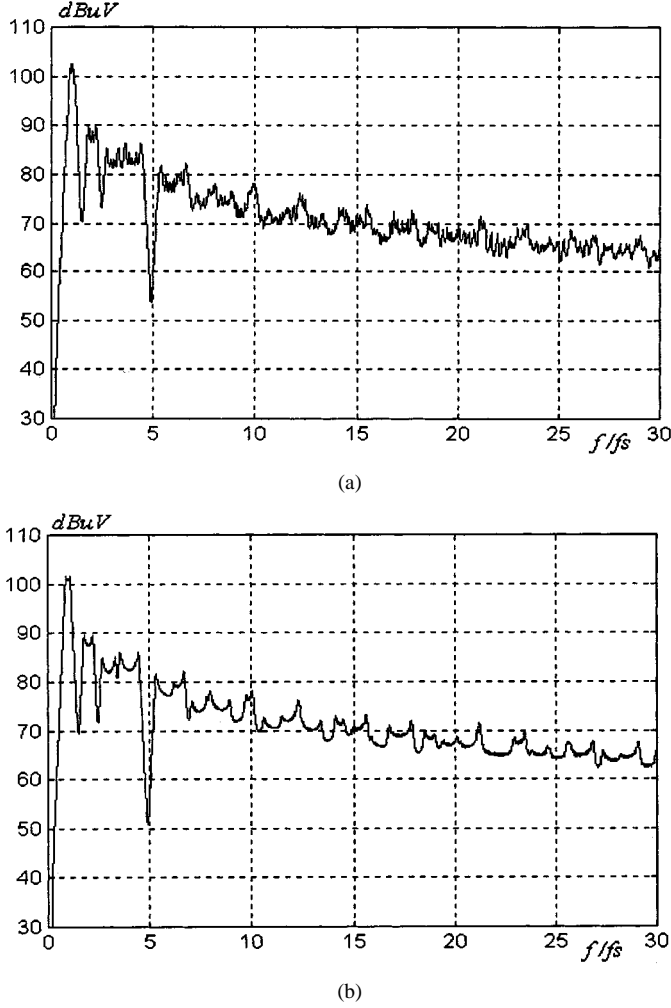


Fig. 9. Comparison of the predicted power spectra with $BW_{res} = 9$ kHz and $\Delta f_s = 12$ kHz. (a) $f_m = 6$ kHz and $\beta = 2$. (b) $f_m = 1.5$ kHz and $\beta = 8$.

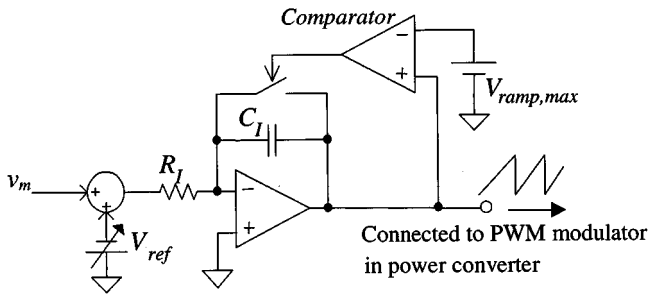


Fig. 10. Implementation of the ramp VCO.

Low-frequency noise will inherently introduce when \mathfrak{R} is nonzero. Selection of \mathfrak{R} is based on the harmonic spreading effects and the low-frequency noise injection.

III. EXPERIMENTAL VERIFICATIONS AND COMPARISONS

The same converter, as tabulated in Table II, is investigated. CFM is achieved by using the ramp voltage-controlled oscillator (VCO) shown in Fig. 10. By integrating the signal that combines a modulating signal v_m (which is either periodic or random) and

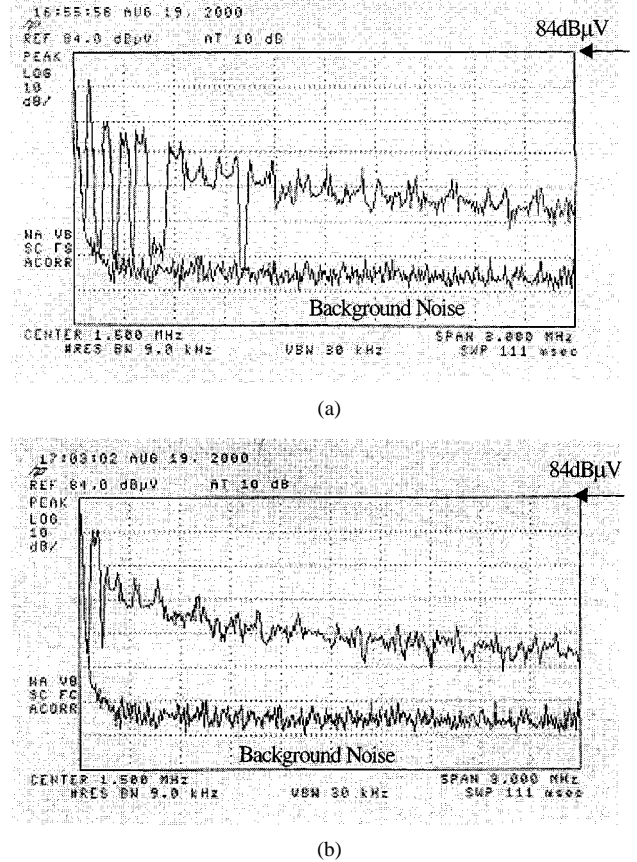


Fig. 11. Measured power spectrum of the input current with PCFM (10 dB/div). (a) $f_m = 3$ kHz, $\Delta f_s = 6$ kHz, and $\beta = 2$. (b) $f_m = 3$ kHz, $\Delta f_s = 24$ kHz, and $\beta = 8$.

a reference dc voltage V_{ref} , a triangular waveform is generated. The peak value $V_{ramp,max}$ of the output is defined as

$$V_{ramp,max} = \frac{1}{R_I C_I} \int_0^{T_s} (-V_{ref} + v_m) dt \quad (26)$$

where T_s is the generated switching period. The modulated switching frequency equals

$$f_s = G_{VCO}(-V_{ref} + v_m) = f_s + \Delta f_s \quad (27)$$

where $G_{VCO} = 1/(R_I C_I V_{ramp,max})$ is the gain of the VCO, $f_s = -G_{VCO} V_{ref}$, and $\Delta f_s = G_{VCO} v_m$.

Fig. 11 shows the measured power spectrum of the input current under PCFM with the same condition as in Fig. 8. The EMC analyzer is an HP 8591EM [13] and BW_{res} equals 9 kHz. The conversion factor of the current probe is 0.05 V/A (which introduces a 26 dB offset in the overall spectrum). As the cutoff frequency of the output filter is 332 Hz, the value of Δf_s satisfies (24). It can be seen that the measured results agree closely with the predictions. In the RCFM, the measured spectrum under the same frequency deviation is examined. The equivalent random level \mathfrak{R} equals $(1/76 - 1/124)/(1/100) = 0.5$. The theoretical and measured results are shown in Fig. 12.

Comparing Fig. 11 with Fig. 12, both PCFM and RCFM give similar profiles in the measured spectra, especially in the high-frequency range. However, for the low-frequency harmonics,

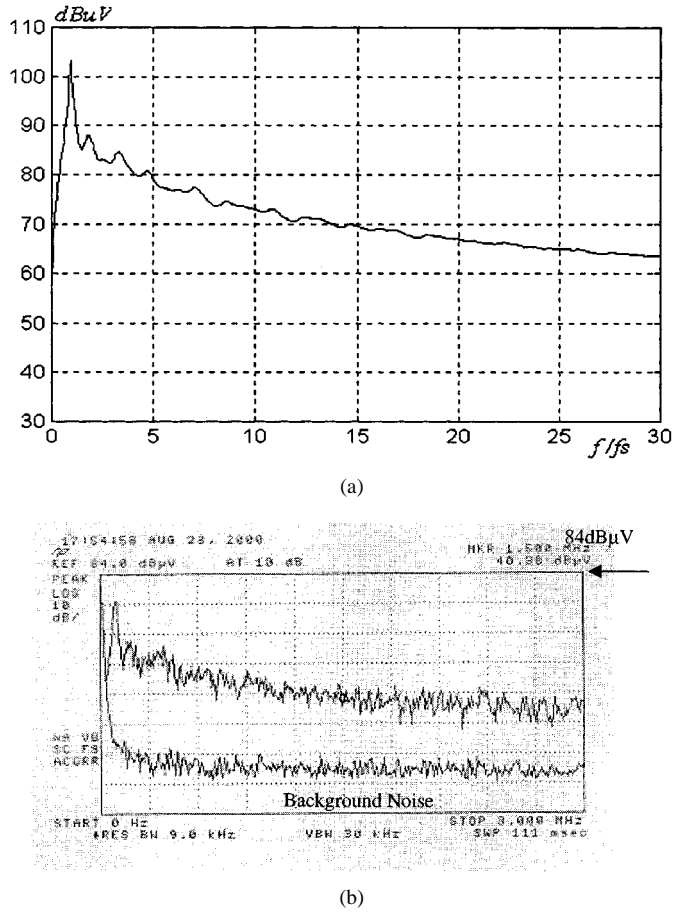


Fig. 12. Power spectra of the input current with RCFM and $BW_{res} = 9$ kHz. (a) Theoretical prediction. (b) Measured result.

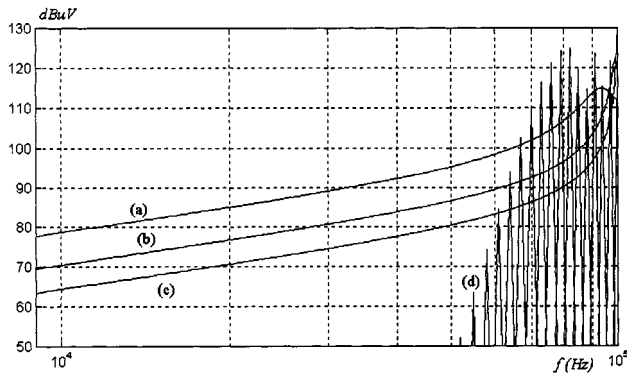


Fig. 13. Comparison of the low-frequency characteristics of the diode voltage with $BW_{res} = 200$ Hz. (a): RCFM, $R = 0.5$. (b): RCFM, $R = 0.2$. (c): RCFM, $R = 0.1$. (d): PCFM.

the performance of the two schemes are different. The theoretical spectra of the diode voltage with the two schemes are shown in Fig. 13. Basically, RCFM gives higher low-frequency harmonics than the PCFM. No harmonics will be generated beyond the sideband of the first-order-switching harmonic in PCFM [Fig. 13(d)]. Fig. 14 shows the output voltage of the converter under the two schemes. It can be observed that the RCFM introduces higher low-frequency variation than the PCFM, thus confirming the theoretical prediction. Although low-frequency harmonics in the RCFM can be reduced with a smaller R [Fig. 13(b)

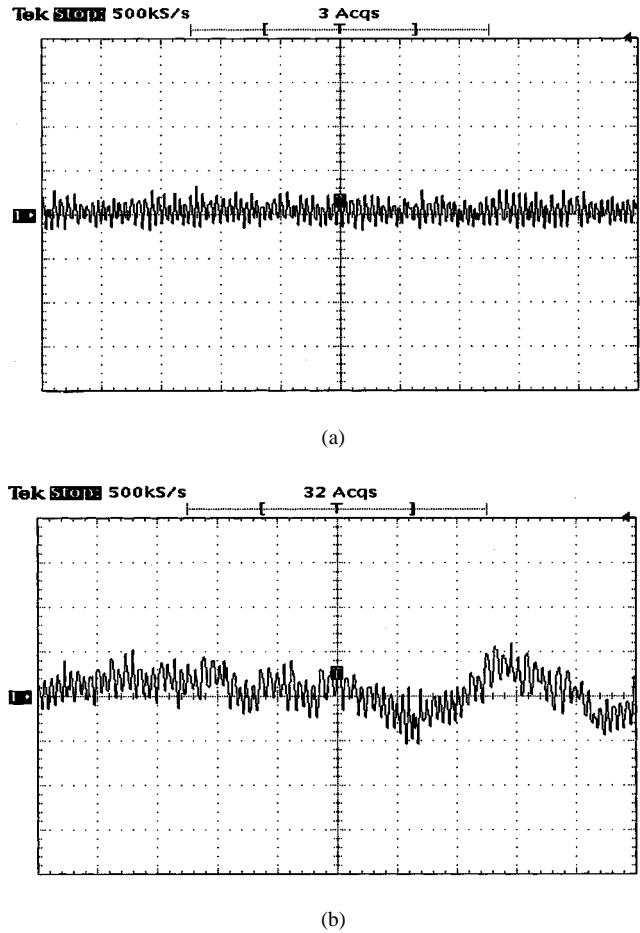


Fig. 14. Measured output ripple (50 mV/div) (timebase: 100 $\mu\text{s}/\text{div}$). (a) PCFM. (b) RCFM.

and (c)], the effectiveness of the frequency spreading will be lowered [6] and the harmonic components around the switching frequency will be increased. Nevertheless, with the same frequency deviation, RCFM gives a more effective way to disperse the harmonics around the switching frequency than the PCFM.

Due to different spectral behaviors of the two schemes, they can be applied to applications of different requirements. PCFM is more suitable for applications that require tight output regulation, like dc/dc converters, since it introduces lower undesirable low-frequency harmonics at the output. On the other hand, RCFM is more suitable for applications that do not require tight output regulation, like power-factor correctors, since output regulation is usually performed in the second stage and high-frequency harmonic suppression is more effective.

IV. CONCLUSION

A comparative study on using PCFM and RCFM schemes for EMI suppression of PWM converters has been presented. Both schemes can provide a considerable reduction in the conducted EMI, as compared to the standard PWM scheme. With the same frequency deviation in both schemes, RCFM gives a higher high-frequency suppression than the PCFM. However, RCFM introduces higher low-frequency harmonics than the PCFM at the converter output. Rigorous mathematical derivations on the spectral characteristics of the PCFM have

been developed. In addition, due to the finite bandwidth of the resolution filter in EMC analyzers, discrepancies between the theoretical and experimental results have been explained. Selections of the modulation frequency and the frequency deviation in PCFM have been discussed. Finally, theoretical predictions are confirmed by experimental results of a buck converter operating in continuous conduction mode.

REFERENCES

- [1] M. D. Heerema, "Designing for electromagnetic compatibility," in *Proc. Hewlett-Packard Seminar*, 1996, pp. 1–29.
- [2] H. Chung, S. Y. R. Hui, and K. K. Tse, "Reduction of power converter EMI emission using soft-switching technique," *IEEE Trans. Electromagn. Compat.*, vol. 40, pp. 282–287, Aug. 1998.
- [3] F. Lin and D. Y. Chen, "Reduction of power supply EMI emission by switching frequency modulation," *IEEE Trans. Power Electron.*, vol. 9, pp. 132–137, Jan. 1994.
- [4] T. G. Habetler and D. M. Divan, "Acoustic noise reduction in sinusoidal PWM drives using a randomly modulated carrier," *IEEE Trans. Power Electron.*, vol. 6, pp. 356–363, July 1991.
- [5] A. M. Stankovic, G. C. Verghese, and D. J. Perreault, "Analysis and synthesis of randomised modulation schemes for power converters," *IEEE Trans. Power Electron.*, vol. 10, pp. 680–693, Nov. 1995.
- [6] K. K. Tse, H. Chung, S. Y. R. Hui, and H. C. So, "A comparative investigation on the use of random modulation schemes for dc/dc converters," *IEEE Trans. Ind. Electron.*, vol. 47, pp. 245–252, Apr. 2000.
- [7] D. Stone and B. Chambers, "The effects of carrier frequency modulation of PWM waveforms on conducted EMC problems in switched mode power supplies," *EPE J.*, vol. 5, no. 3/4, pp. 32–37, Jan. 1996.
- [8] M. Bech, F. Blaabjerg, and J. Pederson, "Random modulation techniques with fixed switching frequency for three-phase power converters," *IEEE Trans. Power Electron.*, vol. 15, pp. 753–761, July 2000.
- [9] C. R. Wylie and L. C. Barrett, *Advanced Engineering Mathematics*. New York: McGraw-Hill, 1995.
- [10] A. B. Carlson, *Communication Systems: An Introduction to Signal and Noise in Electrical Communication*. New York: McGraw-Hill, 1986.
- [11] G. Kennedy, *Electronic Communication Systems*. New York: McGraw-Hill, 1985.
- [12] R. A. Witte, *Spectrum and Network Measurements*. Englewood Cliffs, NJ: Prentice-Hall, 1991.
- [13] *HP8590 EM Series User's Guide*, Hewlett Packard Co., Palo Alto, CA, 1995.



K. K. Tse (M'00) received the B.Eng. (Hons.) degree in electrical engineering from The Hong Kong Polytechnic University, Hong Kong, and the Ph.D. degree from City University of Hong Kong, Hong Kong, in 1995 and 2000, respectively.

He served as a Lecturer at the Hong Kong Institute of Vocational Education (Tsing Yi) (formerly Technical College) in 1998. From 1999 to 2001, he was a Research Fellow in the Electronic Engineering Department, City University of Hong Kong. Since June 2001, he has been with Johnson Electric, Hong Kong,

where he is currently a Technical Specialist in the R&D area. He has authored more than 20 published technical papers in the areas of his research interests, which include new numerical model methods and computer-aided simulation techniques, EMI reduction using random switching schemes for dc–dc converters, and new maximum power tracking techniques for PV cells.

Dr. Tse received the First Prize in 1998 in the IEEE Postgraduate Student Paper Contest, Hong Kong Section, and the Third Prize in the 1999 Region 10 IEEE Postgraduate Student Paper Contest. He was a recipient of The Croucher Foundation Fellowship in 2000. In December 2000, he received the Silver Award in the Young Inventor Competition, jointly organized by the Far Eastern Economic Review and Hewlett Packard Company.



Henry Shu-Hung Chung (S'92–M'95) received the B.Eng. (with first class honors) degree in electrical engineering and the Ph.D. degree from The Hong Kong Polytechnic University, Hong Kong, in 1991 and 1994, respectively.

Since 1995, he has been with City University of Hong Kong, Hong Kong, where he is currently an Associate Professor in the Department of Electronic Engineering. His research interests include time- and frequency-domain analysis of power electronic circuits, switched-capacitor-based converters, random-

switching techniques, digital audio amplifiers, soft-switching converters, and electronic ballast design. He has authored four research book chapters and more than 130 technical papers, including 65 refereed journal papers in the current research area, and is the holder of two U.S. patents.

Dr. Chung is currently the IEEE Student Branch Counselor at City University of Hong Kong and was Track Chair of the Technical Committee on Power Electronics Circuits and Power Systems of the IEEE Circuits and Systems Society in 1997–1998. He is presently an Associate Editor of the IEEE TRANSACTIONS ON CIRCUITS AND SYSTEMS I. He was awarded the Grand Applied Research Excellence Award in 2001 from City University of Hong Kong.



S. Y. Ron Hui (SM'94) was born in Hong Kong in 1961. He received the B.Sc. (Hons.) degree in 1984 from the University of Birmingham, Birmingham, U.K., and the D.I.C. and Ph.D. degree in 1987 from Imperial College of Science and Technology, University of London, London, U.K.

He was a Lecturer in power electronics at the University of Nottingham, Nottingham, U.K., in 1987–1990. In 1990, he took up a lectureship at the University of Technology, Sydney, Australia, where he became a Senior Lecturer in 1991. He joined

the University of Sydney in 1993 and was promoted to Reader of Electrical Engineering and Director of the Power Electronics and Drives Research Group in 1996. He is currently a Chair Professor of Electronic Engineering and an Associate Dean of the Faculty of Science and Engineering at City University of Hong Kong, Hong Kong. He has authored more than 150 published technical papers, including more than 80 refereed journal publications. His research interests include all aspects of power electronics.

Prof. Hui received the Teaching Excellence Award in 1999 and the Grand Applied Research Excellence Award in 2001 from City University of Hong Kong. He has been appointed an Honorary Professor by the University of Sydney since 2000.



H. C. So was born in Hong Kong. He received the B.Eng. degree from City University of Hong Kong, Hong Kong, and the Ph.D. degree from Chinese University of Hong Kong, Hong Kong, in 1990 and 1995, respectively, both in electronic engineering.

From 1990 to 1991, he was an Electronic Engineer in the Research and Development Division, Everex Systems Engineering Ltd. He was then a Post-Doctoral Fellow at Chinese University of Hong Kong for one year. From 1996 to 1999, he was a Research Assistant Professor in the Department of Electronic Engineering, City University of Hong Kong. Currently, he is an Assistant Professor in the Department of Computer Engineering and Information Technology, City University of Hong Kong. His research interests include adaptive filter theory, detection and estimation, wavelet transform, and signal processing for communications and multimedia.